Fermi Surface of $AuSb_2$. II. de Haas–van Alphen and de Haas–Shubnikov Effects*

J. AHN† AND D. J. SELLMYER
Center of Materials Science and Engineering, Massachusetts Institute of Technology, Cambridge, Massachusetts 02139
(Received 30 April 1969; revised manuscript received 6 October 1969)

de Haas–van Alphen and de Haas–Shubnikov oscillations were investigated in {100} and {110} planes of the metallic compound $AuSb_2$. The orientation dependence of eight sets of external Fermi-surface areas was determined. These frequencies ranged from about 8×10^4 G to 5×10^7 G. Where the frequency and cyclotron mass data for the two experiments overlapped, the agreement was excellent. An attempt was made to compare the field dependence of the amplitude of one set of oscillations in the two experiments. The de Haas–Shubnikov data fit the theory for fields below about 75 kG but the de Haas–van Alphen data did not fit the theory for any field range down to about 20 kG, the lowest field at which the latter oscillations could be measured. These anomalies in field dependence seem to be connected with magnetic breakdown but the precise mechanism that could explain the apparently different breakdown fields seen in the two experiments is not clear. Two nearly free-electron models were constructed for the Fermi surface. These models assumed effective valences of 1 for gold and either 5 or 3 for antimony. However, since neither model was capable of explaining the orientation dependence of the extremal areas, it was concluded that the electronic structure of this compound is not nearly free-electron-like.

I. INTRODUCTION

SINCE the discovery of the de Haas–van Alphen (dHvA) and de Haas–Shubnikov (dHS) effects, these phenomena have become very powerful tools in investigating the electronic structure of metals. In the present paper, we report Fermi-surface properties of the metallic compound $AuSb_2$ as investigated by the dHvA and dHS effects. Topological properties of the Fermi sufrace, as determined by high-field magnetoresistance (MR) measurements, were reported in the first paper in this series, hereafter referred to as I.[1]

As explained in I, at present there have been Fermi-surface determinations and energy-band calculations for a number of metallic compounds having the cesium-chloride,[2,3] fluorite,[4,5] and nickel-arsenide[6–8] structures. The purpose of this program of research is to gain insight into the nature of the quantum chemistry of the class of solids whose chemical binding forces cannot be characterized clearly as ionic, covalent, or metallic. There is the fundamental question as to whether the present form and calculational technique of band theory is sufficiently powerful to handle crystal structures having more than three or four atoms per primitive cell, especially in those cases where there may be significant charge transfer. The alternative approach is a semi-empirical, valence-bond method such as the one advanced by Pauling.[9] There is the further interesting question as to the meaning of the quantities that enter the latter theory in terms of the actual band structure of the solid. As an example, Pauling has given a discussion of the quantum chemistry of the NiAs structure compound AuSn.[10] The essential feature of it is that there are 1.56 metallic orbitals (conduction electrons) per atom of gold while the other valence electrons of the gold and tin atoms go into covalent bonds. In terms of this theory, then, one would expect about three conduction electrons per primitive cell for AuSn since each cell has two units of AuSn. However, recent dHvA[8] and high-field MR[7] results indicate that the Fermi surface of AuSn is similar to the nearly free-electron (NFE) model which is based on *ten* almost free electrons per primitive cell. The relationship between the two descriptions of AuSn, if any, is not clear.

A study of the Fermi surface of $AuSb_2$ was further motivated by the rather surprising success of the NFE model in explaining the Fermi surfaces of several compounds having some of the simpler crystal structures In particular, the NFE nature of several compounds based on gold, viz., AuSn and AuX_2, where X is Al, Ga, or In,[4–8] suggested that it would be interesting to further test this model in a compound having a somewhat more complicated crystal structure than the above-mentioned ones.

The organization of this paper is as follows. Section II consists of some major results from the theories of

* Research supported by the Advanced Research Projects Agency and performed in part at the Francis Bitter National Magnet Laboratory which is supported by the U. S. Air Force Office of Scientific Research.
† IBM Graduate Fellow. Present address: IBM, East Fishkill Facility, Hopewell Junction, N. Y.
[1] J. Ahn and D. J. Sellmyer, preceding paper, Phys. Rev. B **1**, 1273 (1970).
[2] D. J. Sellmyer, J. Ahn, and J.-P. Jan, Phys. Rev. **161**, 618 (1967); J.-P. Jan, W. B. Pearson, and Y. Saito, Proc. Roy. Soc. (London) **A297**, 275 (1967); A. Beck, J.-P. Jan, W. B. Pearson, and I. M. Templeton, Phil. Mag. **8**, 351 (1963).
[3] K. H. Johnson and H. Amar, Phys. Rev. **139**, A760 (1965); H. Amar, K. H. Johnson, and K. P. Wang, *ibid.* 148, 672 (1966); F. J. Arlinghaus, *ibid.* **157**, 491 (1967); Intern. J. Quantum Chem. **15**, 605 (1967).
[4] J. T. Longo, P. A. Schroeder, and D. J. Sellmyer, Phys. Letters **25A**, 747 (1967); Phys. Rev. **182**, 658 (1969); J.-P. Jan, W. B. Pearson, Y. Saito, M. Springford, and I. Templeton, Phil. Mag. **12**, 1271 (1965).
[5] A. C. Switendick, Bull. Am. Phys. Soc. **15**, 360 (1969).
[6] D. J. Sellmyer and P. A. Schroeder, Phys. Letters **16**, 100 (1965).
[7] D. J. Sellmyer, J. Phys. Chem. Solids **30**, 2371 (1969).
[8] G. J. Edwards, M. Springford, and Y. Saito, J. Phys. Chem. Solids **30**, 2527 (1969).
[9] L. Pauling, *The Nature of the Chemical Bond* (Cornell University Press, Ithaca, N. Y., 1960), 3rd ed.
[10] L. Pauling, Ref. 9, p. 422.

the dHvA and dHS effects and magnetic breakdown. The experimental techniques used in the measurements are described in Sec. III. In Sec. IV, the frequency results are presented first, followed by a comparative study of amplitudes in the two types of oscillations. Section V contains a discussion of the observed amplitude anomalies along with a comparison of the frequency results with the NFE Fermi-surface model. The concluding remarks are found in Sec. VI.

II. THEORY

A. Quantum Oscillatory Effects

The theory of the dHvA effect has been given by Lifshitz and Kosevich,[11] and recently theoretical and experimental aspects of the effect have been comprehensively reviewed by Gold.[12] With the effects of spin and collisions taken into account,[13] and with the field **B** in the z direction, the oscillatory magnetization arising from a single extremal area A_m of the Fermi surface may be written as[14]

$$M_{\rm osc}=\left(\frac{2\pi F}{B}\right)B^{1/2}T \times\sum_{r=1}^{\infty}\frac{P_r e^{-rT_D/T_B}\cos[2\pi r(F/B)\mp\frac{1}{4}\pi-2\pi r\gamma]}{r^{1/2}\sinh[r(T/T_B)]}, \quad (1a)$$

where

$$P_r=-2k_B\left(\frac{e}{hc}\right)^{3/2}\left|\frac{\partial^2 A_m(\epsilon_F)}{\partial k_z^2}\right|^{-1/2}\cos\left(\frac{1}{2}r\pi g\frac{m_c}{m_0}\right), \quad (1b)$$

$$F=\hbar cA_m(\epsilon_F)/2\pi e, \quad (1c)$$

$$T_B=e\hbar B/2\pi^2 k_B m_c c, \quad (1d)$$

$$T_D=\hbar/2\pi k_B\tau. \quad (1e)$$

In the above, γ is a phase constant which may have any value between 0 and $\frac{1}{2}$ depending on the $E(\mathbf{k})$ relationship, F is the dHvA frequency, T_D is the Dingle or scattering temperature, τ is the electronic relaxation time, m_c is the cyclotron mass, ϵ_F is the Fermi energy, and the other symbols have their usual meanings. In many cases of interest, $T/T_B\gg1$ so that only the term $r=1$ is significant. Then all terms with $r>1$ in Eq. (1a) can be neglected and it becomes

$$M_{\rm osc}=K\frac{T}{B^{1/2}}\frac{e^{-T_D/T_B}}{\sinh(T/T_B)}\cos\left(\frac{2\pi F}{B}+\phi\right), \quad (2)$$

where K and ϕ are constants.

Quantum oscillations in the MR, the dHS effect, were first observed in Bi by dHS.[15] Fundamental papers on the theory of this effect are those of Lifshitz and Kosevich[16] and Adams and Holstein.[17] Recently, the subject has been reviewed by Kahn and Fredrikse[18] and Roth and Argyres.[19] The most extensive experimental study of the dHS effect was done by Soule *et al.*[20] in graphite. This work verified the essential validity of the theory of Adams and Holstein.

The case of the dHS effect for a spherical Fermi surface and transverse geometry has been discussed by Yep and Becker.[21] From their results, it can be shown that when $T/T_B\gg1$, the field and temperature dependence for the DHS oscillations is identical to that given for $M_{\rm osc}$ in Eq. (2). Thus it should be possible to employ either effect to determine extremal areas, cyclotron masses, and Dingle temperatures.

The amplitude of the dHS effect may be estimated[22] by the free-electron theory:

$$\delta\sigma/\sigma\simeq(2\nu)^{-1/2}, \quad (3)$$

where ν corresponds to the quantum number associated with the Landau level at the extremal Fermi-surface area A_m at the field B_ν; ν is given by $\nu\simeq\nu+\gamma=\hbar cA_m/2\pi eB_\nu=F/B_\nu$. Equation (3) predicts that the ratio of the oscillatory conductivity amplitude to the steady (nonoscillatory) part is proportional to $\sqrt{(B/F)}$, so $\delta\sigma/\sigma$ is expected to be large for small orbits at high fields. Qualitatively, this prediction agrees with the experimental observation that large-amplitude dHS oscillations are easily observable in the semimetals Bi [23] and Sb.[24] However, this simple estimate appears to fail when applied to a common metal whose Fermi surface consists of large as well as small pieces. In such cases, it has been suggested[7] that the larger pieces of Fermi sur-

[11] I. M. Lifshitz and A. M. Kosevich, Zh Eksperim. i Teor. Fiz. **29**, 730 (1955) [English transl.: Soviet Phys.—JETP **2**, 636 (1956)].

[12] A. V. Gold, in *Solid State Physics*, edited by J. F. Cochran and R. R. Haering (Gordon and Breach, Science Publishers, Inc., New York, 1968), Vol. I.

[13] R. B. Dingle, Proc. Roy. Soc. (London) **A211**, 517 (1952); M. H. Cohen and E. I. Blount, Phil. Mag. **5**, 115 (1960).

[14] In a nonmagnetic metal like $AuSb_2$, the difference between **B** and **H** is usually so small that the two fields can be used interchangeably. **B** is used exclusively in Eq. (1) and in the remainder of this paper.

[15] W. de Haas and L. Shubnikov, Proc. Amsterdam Acad. **33**, 418 (1930); Leiden Commun. 207, 210 (1930).

[16] I. M. Lifshitz and A. M. Kosevich, Zh. Eksperim. i Teor. Fiz. **33**, 88 (1957) [English transl.: Soviet Phys.—JETP **6**, 67 (1958)]; J. Phys. Chem. Solids **4**, 1 (1958).

[17] E. N. Adams and T. D. Holstein, J. Phys. Chem. Solids **10**, 254 (1959).

[18] A. H. Kahn and H. P. R. Frederikse, in *Solid State Physics*, edited by F. Seitz and D. Turnbull (Academic Press Inc., New York, 1959), Vol. IX, p. 257.

[19] L. M. Roth and P. N. Argyres, in *Semiconductors and Semimetals*, edited by R. K. Willardson and A. C. Beer (Academic Press Inc., New York, 1966), Vol. I, p. 159.

[20] D. E. Soule, J. W. McClure, and L. B. Smith, Phys. Rev. **134**, A453 (1964).

[21] T. O. Yep and W. M. Becker, Phys. Rev. **144**, 741 (1966).

[22] A. B. Pippard, *The Dynamics of Conduction Electrons* (Gordon and Breach, Science Publishers, Inc., New York, 1965), p. 109.

[23] C. G. Grenier, J. M. Reynolds, and J. R. Sybert, Phys. Rev. **132**, 58 (1963).

[24] G. N. Rao, N. H. Zebouni, C. G. Greiner, and J. M. Reynolds, Phys. Rev. **113**, A141 (1964).

face effectively short circuit the oscillations from the small pieces of Fermi surface, and that the estimate of Eq. (3) will be limited by the largest pieces of Fermi surface. For example, if $F=10^8$ G, $B=10^5$ G, then $\delta\sigma/\sigma$ is only about 1%.

B. Magnetic Breakdown

Magnetic breakdown is known to modify the amplitude of the oscillatory effects. The effects of breakdown were first observed by Dhillon and Shoenberg[25] in their dHvA study of Zn, but recently it has been shown[26] that the observed dHvA amplitude can be modified by a field-dependent breakdown factor, so that the corrected amplitude obeys the field dependence predicted by Eq. (2). In explaining the MR oscillations in Zn, Stark[27] theorized that the unusually large amplitudes ($\delta\sigma/\sigma\simeq 1$) were due to an oscillating breakdown probability P [28] [see Eq. (3) of I], caused by the oscillating *effective* energy gap across which the breakdown took place. Recent theoretical papers on the effects of breakdown on quantum oscillatory phenomena are those of Falicov and co-workers[29] and a general review of magnetic breakdown in metals has been given by Stark and Falicov.[30]

III. EXPERIMENTAL TECHNIQUES

A. Specimen and Magnetic-Field Considerations

The crystal growth of $AuSb_2$ samples has been described in I. Samples for oscillatory MR experiments were identical to those used in the ordinary high-field MR experiments. Samples for dHvA experiments were spark-cut from the Czochralski crystal exclusively. Cylindrical samples (0.25×0.4 cm) with their axes oriented in ⟨100⟩, ⟨110⟩, and ⟨111⟩ directions were spark-cut by the method described in I. One end of each sample was spark-planed accurately so that it was normal to the axis of the sample. A total of six samples of of the above orientations were shaped for dHvA experiments.

As in I, all experimental results were obtained with 5.1-cm bore water-cooled solenoids providing a maximum field of 150 kG. The long-term field stability was ~0.01% but there was present ~0.1% of 6 Hz ripple from the 24 000-A current source. The field was calibrated to ~0.2%. The ac field ripple was effectively eliminated in the dHvA experiments by a superconducting low-pass filter which has been described previously.[31] The field homogeneity of the "high-homogeneity" magnet, exclusively used for dHvA experiments, was better than 0.01% over 4 cm. The requirement for a high homogeneity in the dHvA effect arises from the fact that, as given by Eq. (2), the argument of the cosine term varies as $2\pi F/B$. Substituting the highest frequency observed in this work, $F=5\times10^7$ G, and $B=100$ kG, we have $2\pi F/B\simeq\pi\times10^3$. This means that the field homogeneity, expressed as $\Delta B/B$ must be smaller than $\sim10^{-3}$ over the sample volume for this frequency to be observable. Therefore, with the available field homogeneity and a sample of linear dimensions $\lesssim$4 cm, it would be possible to observe a frequency of the order of 5×10^8 G.

B. dHS Effect

MR oscillations were observed either in dc as described in I if the amplitude was large, or with a field-modulation technique.[32] In the dc method, the steady part of the MR was bucked out by means of a variable attenuator. In the field-modulation technique, a 10-Hz modulation field of magnitude up to 1 kG was derived by modulating the main magnet current. Figure 1 shows a block diagram of the electronic apparatus. With a constant sample current between 1 and 2 A, an ac signal was induced at the transformer secondary (PAR, model AM-1). The ac signal was amplified by the PAR CR-4 and the synchronous detection of this signal, at various multiples of the modulation frequency, was performed with a PAR JB-4 phase-sensitive detector (PSD). The PSD was operated in the selective external mode with a Hewlett Packard Oscillator (model 200 CDR) supplying the reference signal to the PSD. The reference signal was first fed to a frequency multiplier for the second or fourth harmonic detection. The output signal from the PSD was fed to one channel of a Moseley Recorder (model 7100 B). A signal proportional to the magnitude of the field was recorded simultaneously on the chart paper by the second channel of the recorder; this signal was derived from an isolation amplifier of the magnet control console. In this way, any portions of field sweeps which were spurious were detected easily in the recorded traces.

C. dHvA Effect

dHvA oscillations were measured with the field-modulation technique which was introduced by Shoenberg and Stiles[33] and developed by several other

[25] J. S. Dhillon and D. Shoenberg, Phil. Trans. Roy. Soc. London **A248**, 1 (1955). See also R. J. Higgins and J. A. Marcus, Phys. Rev. **161**, 589 (1967).
[26] M. H. Cohen and L. M. Falicov, Phys. Rev. Letters **7**, 231 (1961); A. B. Pippard, Phil. Trans. Roy. Soc. London **A256**, 317 (1964); R. G. Chambers, Proc. Phys. Soc. (London) **88**, 701 (1966).
[27] R. W. Stark, Phys. Rev. Letters **9**, 482 (1962).
[28] E. I. Blount, Phys. Rev. **126**, 1636 (1962).
[29] A. B. Pippard, Proc. Roy. Soc. (London) **A270**, 1 (1962); L. M. Falicov and H. Stochowiak, Phys. Rev. **147**, 505 (1966); L. M. Falicov, A. B. Pippard, and P. R. Sievert, *ibid.* **151**, 499 (1966).
[30] R. W. Stark and L. M. Falicov, in *Progress in Low Temperature Physics*, edited by C. J. Gorter (North-Holland Publishing Co., Amsterdam, 1967). Vol. V, p. 235.
[31] I. S. Goldstein and P. J. Tobin, Rev. Sci. Instr. **40**, 172 (1969).
[32] See, for example, R. W. Stark and L. R. Windmiller, Cryogenics **8**, 272 (1968).
[33] D. Shoenberg and P. J. Stiles, Proc. Roy. Soc. (London) **A281**, 62 (1964)

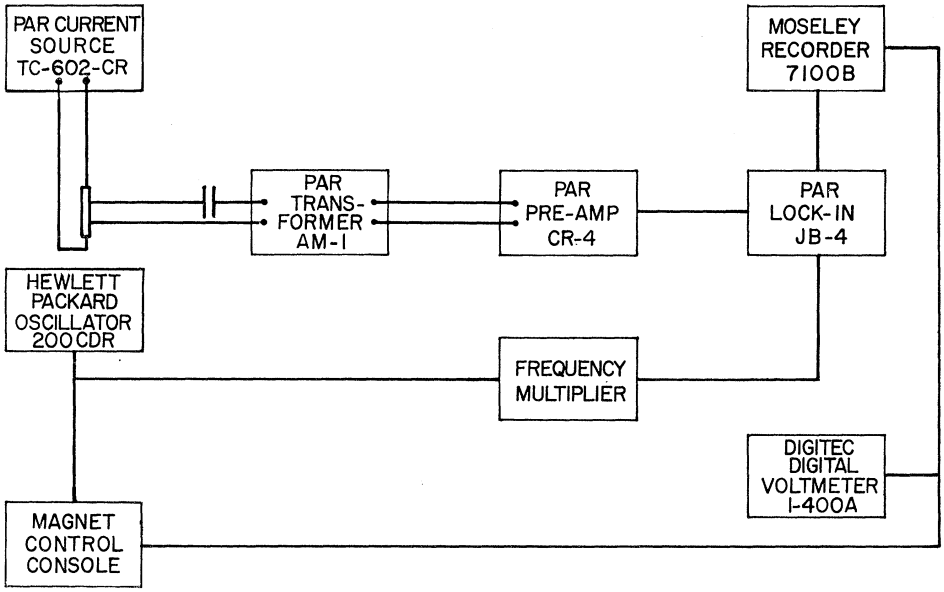

FIG. 1. Block diagram of the electronic apparatus used for detecting oscillatory magnetoresistance by a field-modulation technique. The modifications of the apparatus for dHvA signal detection are discussed in the text.

workers.[34] In essence, a small ac field is superimposed on a large dc magnetic field. The sample is made the core of the transformer in which the field is modulated with frequency ω at the transformer primary and a signal of frequency $n\omega$ (n is an integer) is generated in a pickup coil (transformer secondary) around the sample because of the nonlinear field dependence of the magnetization.

For the dHvA experiment, the block diagram shown in Fig. 1 was modified as follows. An ac signal from the pickup coil was fed to a null twin-tee tuned at the fundamental frequency and the output of the twin-tee was fed to the CR-4 or directly to the PSD, depending on the signal amplitude. The oscillator, in addition to supplying the reference signal to the PSD, supplied the driving signal to an 80-W McIntosh power amplifier which drove the modulation coil. The modulation current was monitored with an rms voltmeter across a 10-Ω resistor in series with the modulation coil. With a 0.1-sec response time of the PSD, the noise level at the detection frequency of 200 Hz from the pickup coil was typically between 0.01 and 0.1 μV. The major source of this noise was the vibration of the sample holder relative to the field. The Bitter solenoids require large amounts of water for cooling and this causes the magnet and Dewar to vibrate somewhat.

The experiments consisted of measuring extremal areas of Fermi surface and their angular dependence in {100} and {110} planes. In order to accomplish this with a few samples, a sample rotator was made which is shown disassembled in Fig. 2(a) and partially assembled in Fig. 2(b). Briefly, an oriented crystal was placed in the pickup coil bobbin E, which was then glued into the rotator D. The rotator was meshed into the spiral gear G which was connected to a turns counting dial at the top of the cryostat by a stainless-steel rod, and two screws F tightly secured D along the axis of rotation. On form B, the modulation coil was wound so that its center coincided with the sample position. On top of the modulation coil a small bifilar-wound copper-wire magnetoresistance probe was attached. This probe was used at the beginning of a run to locate the center of the field to ± 2 mm. A superconducting low-pass filter[31] was mounted on the form A. Three phosphor-bronze springs C were screwed on top of part A to hold the sample assembly rigidly in the stainless-steel Dewar tail. Thus, Fig. 2(b) shows the rotator in place with part B inside part A ready to be slipped over the rotating assembly. The parts A, B, D, E, F, and G were machined from "G-11," which is a glass-cloth-filled Epoxy resin[35] which has a relatively low-expansion coefficient (0.4×10^{-5} per °C) and low water-absorption characteristics. Individual parts of this apparatus are described in detail elsewhere.[36]

Most data were taken with 100-Hz modulation to avoid 60 Hz and its harmonics. At this frequency, the penetration depth in the sample is estimated to be ~ 2 mm at zero field and larger at higher fields due to the MR of the sample.

[34] See, for example, A. Goldstein, S. J. Williamson, and S. Foner, Rev. Sci. Instr. **36**, 1356 (1965); L. R. Windmiller and J. B. Ketterson, *ibid.* **39**, 1672 (1968); Ref. 32.

[35] Purchased from Commercial Plastics and Supply Corp., Cambridge, Mass.

[36] J. Ahn, Ph.D. thesis, Massachusetts Institute of Technology, 1968 (unpublished).

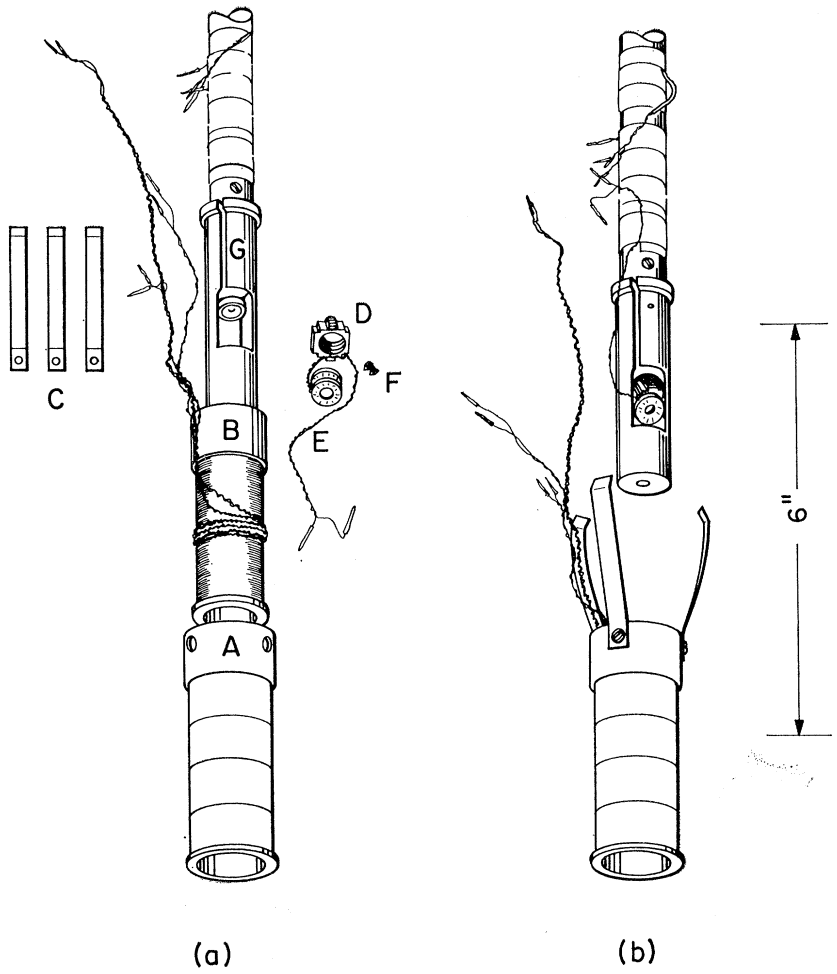

FIG. 2. dHvA sample holder. (a) Disassembled. An oriented crystal is placed in the pickup coil bobbin E, which is glued into the rotator D. The rotator is meshed into the spiral gear G which is connected to a turns counting dial at the top of the cryostat by a stainless-steel rod (not shown); two screws F tightly secure D along the axis of rotation. On form B, the modulation coil is wound so that its center coincides with the sample position. A superconducting low-pass filter is mounted on the form A. Three springs C are screwed on top of A to hold the sample assembly rigidly in the stainless-steel Dewar tail. (b) Partially assembled. D in place with B inside A ready to be slipped over the rotating assembly.

IV. RESULTS

A. dHvA and dHS Frequency Results

Figure 3 shows the angular dependences of all extremal Fermi-surface areas observed with the dHvA and dHS effects. The angle measured from ⟨100⟩ in a {100} plane ({110} plane) is designated as $\theta(\eta)$. Figure 4 shows more clearly the connectivity of data points and the presence of beats. The frequencies are designated as F_i ($i=1$–8) in decreasing order of the magnitude of F. The superscripts α and β in F_1 designated the corresponding oscillations in $\{100\}_\alpha$ and $\{100\}_\beta$ planes, respectively, as defined in I. The prime is used to indicate a frequency F_i', which beats with F_i for $i=2$, 5. In Fig. 4, solid lines are used when sufficient data points assure them. Dashed lines are used when frequencies are present but their magnitudes could not be determined accurately either because of complex beat waveforms or large uncertainties in locating the peaks.

Figures 5 and 6 represent typical dHvA oscillations from which the data points in Fig. 3 were obtained. In these figures, the second harmonic-detection signal is labeled as $V_{2\omega}$. We wish to point out the following features of the dHvA data exhibited in Figs. 3–6:

(1) The frequencies shown in Figs. 3 and 4 are all fundamental dHvA frequencies. In an early experiment in fields up to 150 kG, a frequency of $\sim 9\times 10^7$ was observed but a careful examination showed that this was the second harmonic of F_1. Since F_1 was observable below 100 kG, all subsequent dHvA data were taken in fields up to only 100 kG. Since F_1 itself was close to $2F_2$ for certain directions, it was necessary to consider whether F_1 was the second harmonic of F_2. However, the quantity F_1-2F_2 was greater than the total experimental uncertainty in F_1-2F_2 throughout the angular ranges of θ and η.

(2) F_1^α and F_1^β are the F_1 oscillations observed in the two types of {100} planes in the pyrite structure as explained in I. These two planes are inequivalent crystallographically and this can be expected to show up in the energy bands and dHvA frequencies. However, it is interesting to note that the difference in the two {100}-type planes manifested itself only in the F_1 oscillations and not in the smaller frequencies. This would

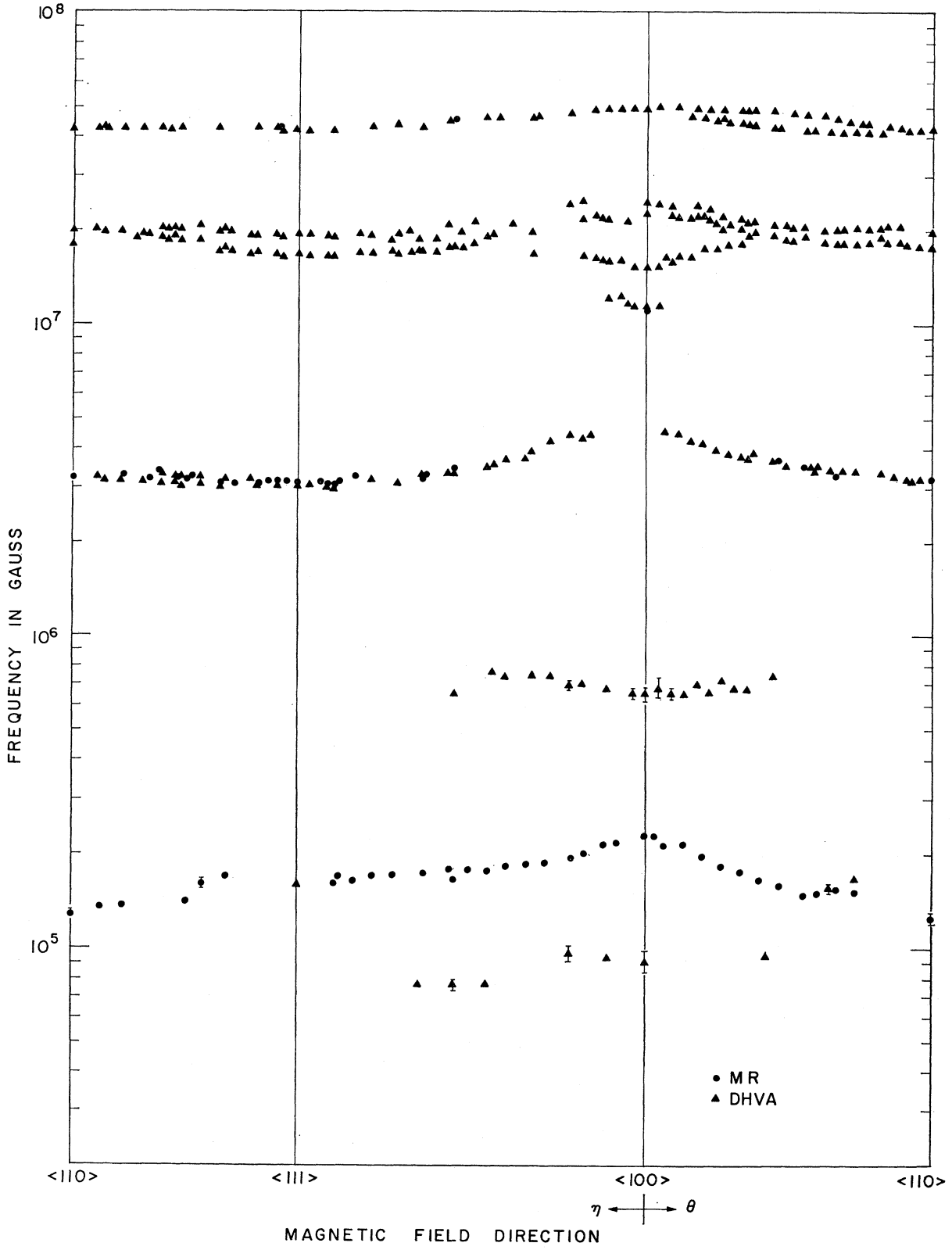

FIG. 3. dHvA (▲) and oscillatory MR (●) frequencies versus magnetic-field directions in {100} and {110} planes.

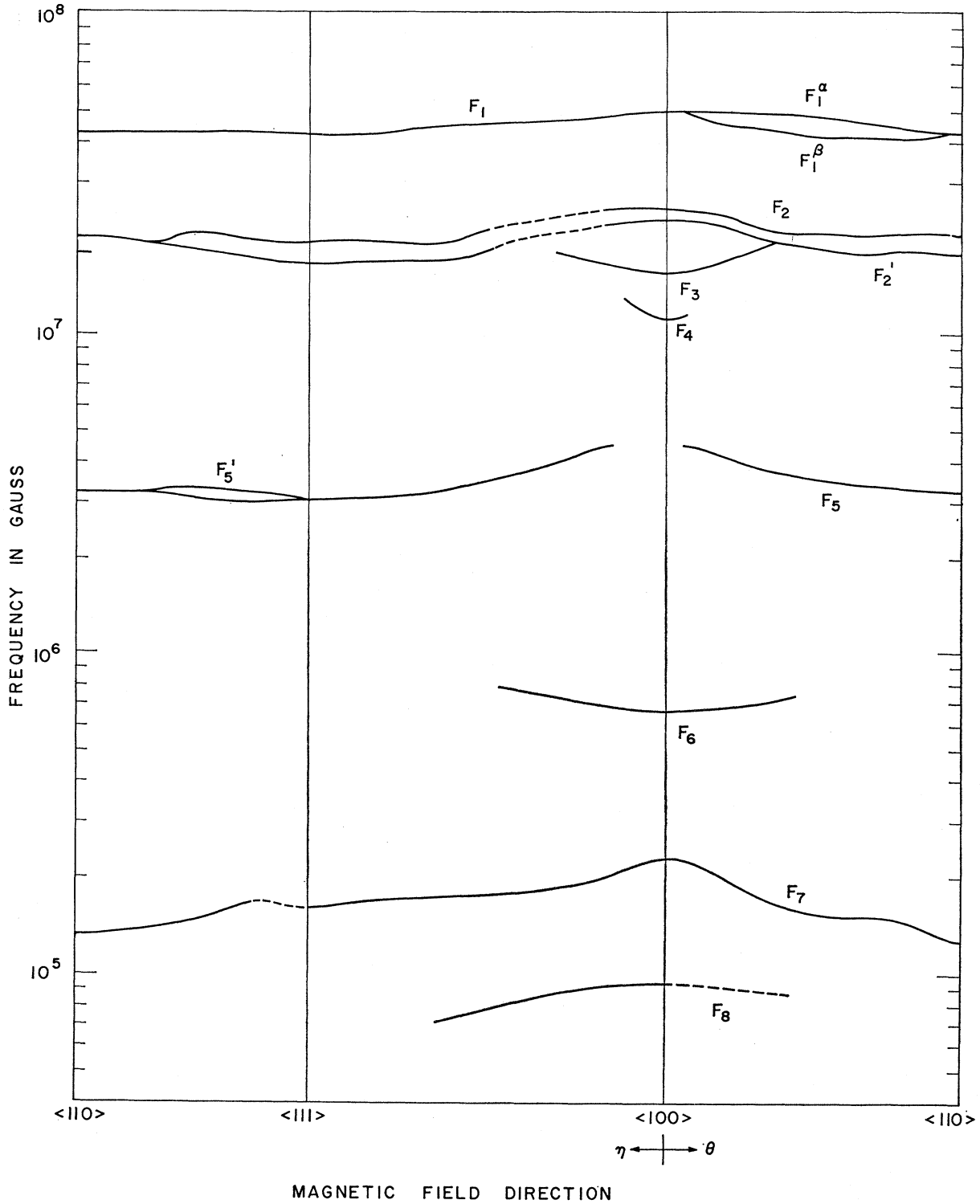

FIG. 4. dHvA and oscillatory MR frequencies versus magnetic-field directions in {100} and {110} planes. This figure shows the connectivity of data points in Fig. 3, labels the frequencies, and shows the presence of beats.

suggest that the smaller pieces of Fermi surface are not situated close to the Brillouin-zone boundaries.

(3) The F_4 oscillations appeared as the dominant frequency of a beat with F_3. Its angular extent was $0°\leq\eta\leq 6°$ and $0°\leq\theta\leq 2°$; these field direction limits correspond almost exactly to the directions for which

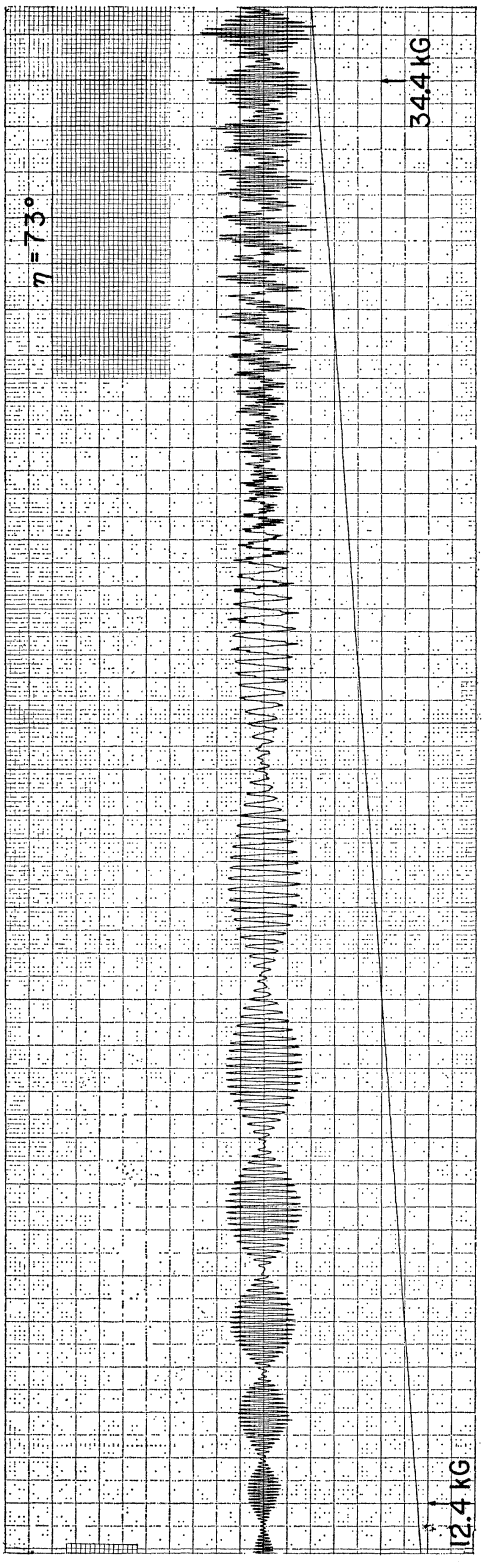

FIG. 5. dHvA oscillation second-harmonic signal at $\eta = 73°$ showing F_5 and F_5' in the low-field region and F_2 and F_2' in the high-field region.

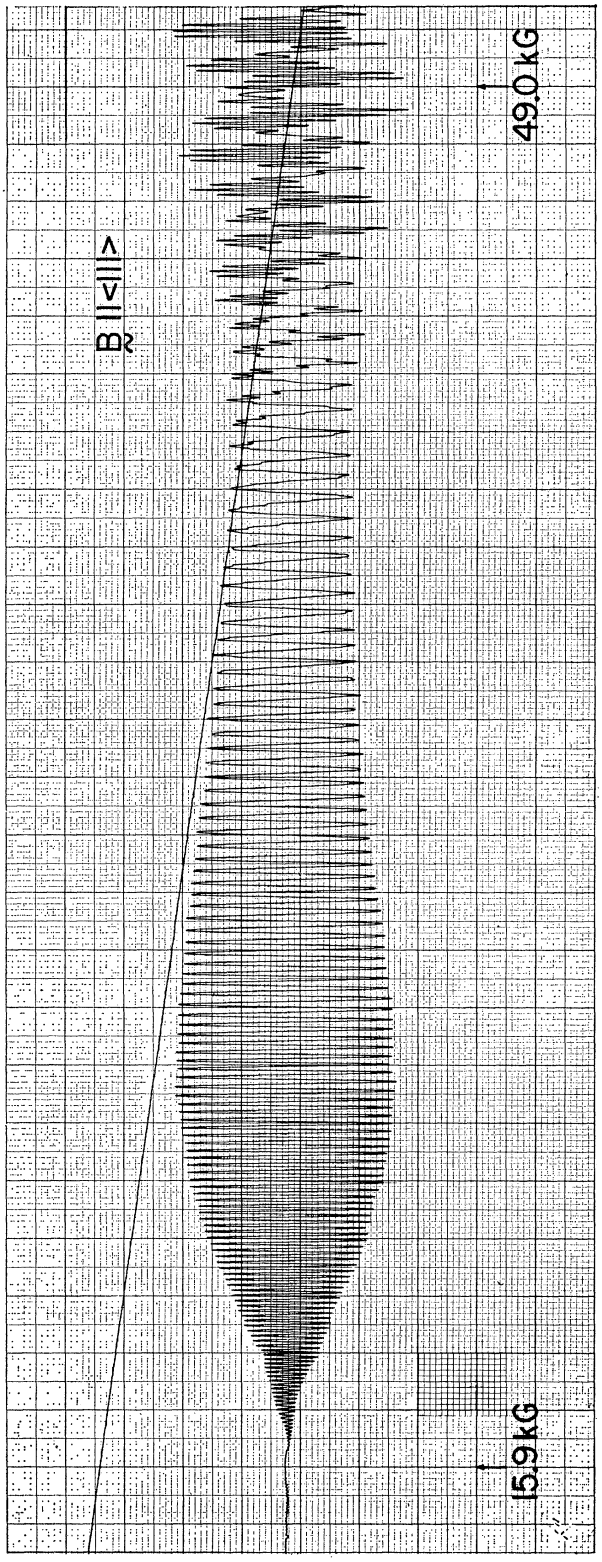

FIG. 6. Second-harmonic dHvA oscillation trace for $\mathbf{B}\|\langle 111\rangle$ near 16 kG, F_5 goes through a Bessel function zero. F_2 is superimposed on F_5 on the high-field side.

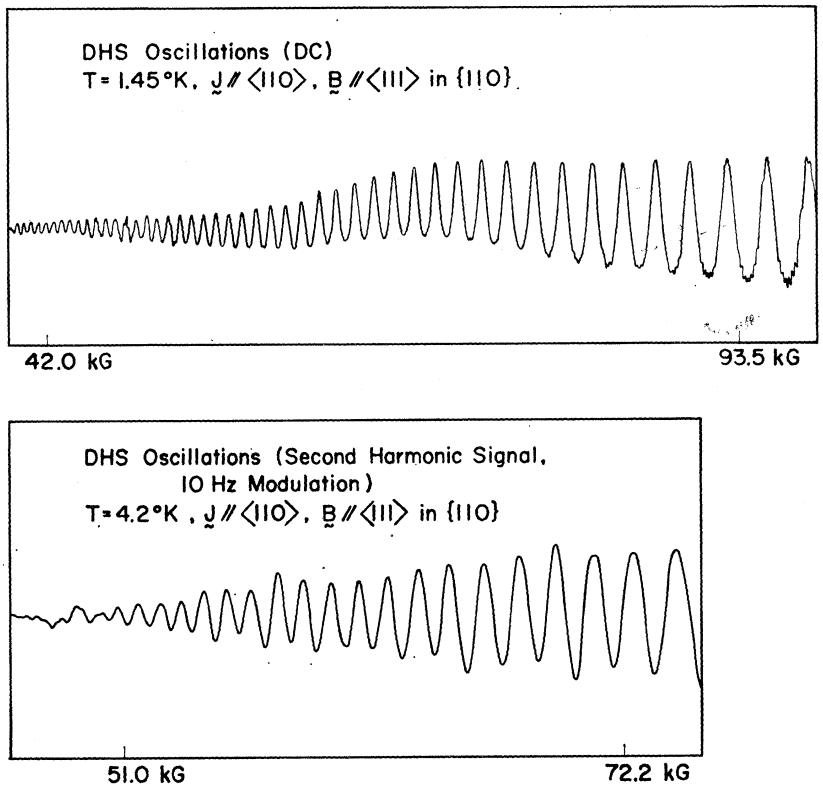

FIG. 7. Typical MR oscillation traces. (a) F_5 recorded by a dc technique; (b) F_5 recorded by the field-modulation technique.

F_5 appeared. This strongly suggests that F_4 and F_5 represent extrema from the same piece of Fermi surface.

(4) The F_5 and F_5' oscillations were carefully investigated by both the dHvA and dHS effects as shown in Fig. 3. Typical dHvA oscillations are shown in the lower-field regions of Figs. 5 and 6. The amplitude anomalies observed when $\mathbf{B}\|\langle 111\rangle$ in both dHvA (Fig. 6) and dHS oscillations are discussed in Sec. IV B.

(5) The F_6, F_7, and F_8 oscillations were observed in the low-field region, typically below 10 kG. Since the number of observed oscillations was small and in a narrow-field range, the accuracy of the frequency determination was relatively poor as indicated by the error bars in Fig. 3; the length of the error bars shows the scatter in frequencies determined from separate runs. Most of the F_7 frequency data was derived from MR oscillations as discussed below.

(6) The dHvA data for $\mathbf{B}\|\langle 100\rangle$ reported by Beck *et al.*[2] are in good agreement with the results from the present work. They reported dHvA frequencies for this single-field direction corresponding to our F_1, F_2, F_3, F_6, and $2F_8$.

Typical examples of MR oscillations as observed in dc or by the field-modulation method are shown in Fig. 7. In the dc trace [Fig. 7(a)] the monotonically varying part of the MR has been bucked out. Both traces show the F_5 oscillations at $\langle 111\rangle$ with a small-amplitude higher frequency (F_1) visible in (a). Because of their relatively large amplitude, the F_5 MR oscillations were chosen for a comparative amplitude study with those of the dHvA effect. The results are described in Sec. IV B.

The F_7 oscillations were observed, in most cases, in the high-field MR experiments. Typically, F_7 appeared as two or three oscillatory peaks superimposed on the steady MR up to 150 kG. [See Figs. 5(a) and (d) of I, for example.] F_7 is maximum when $\mathbf{B}\|\langle 100\rangle$ and was found to exist throughout {100} and {110} planes as shown in Figs. 3 and 4; in the dotted region F_7 was present but the frequency could not be determined accurately because of large uncertainties in locating the peaks. The characteristic feature of F_7 was the shape of the oscillatory peaks in various field orientations. For example, it appeared as "depressions" *below* the steady part of MR as shown in Fig. 5(d) of I. It also appeared as "humps" *above* the steady part of MR as shown in Figs. 5(a) and 3(c) of I. In the latter case, the amplitude of the humps was unusually large, i.e., $\Delta\rho_{\rm osc}/\rho \simeq 0.4$. It is quite likely that these large MR oscillations are caused by magnetic breakdown as discussed in I.

B. Amplitude Studies

As discussed in Sec. II A, the amplitude of dHvA and MR oscillations depends upon the cyclotron mass and the Dingle temperature. Since we have observed both types of oscillations in the same metal it was of interest to compare m_c and T_D as determined by both

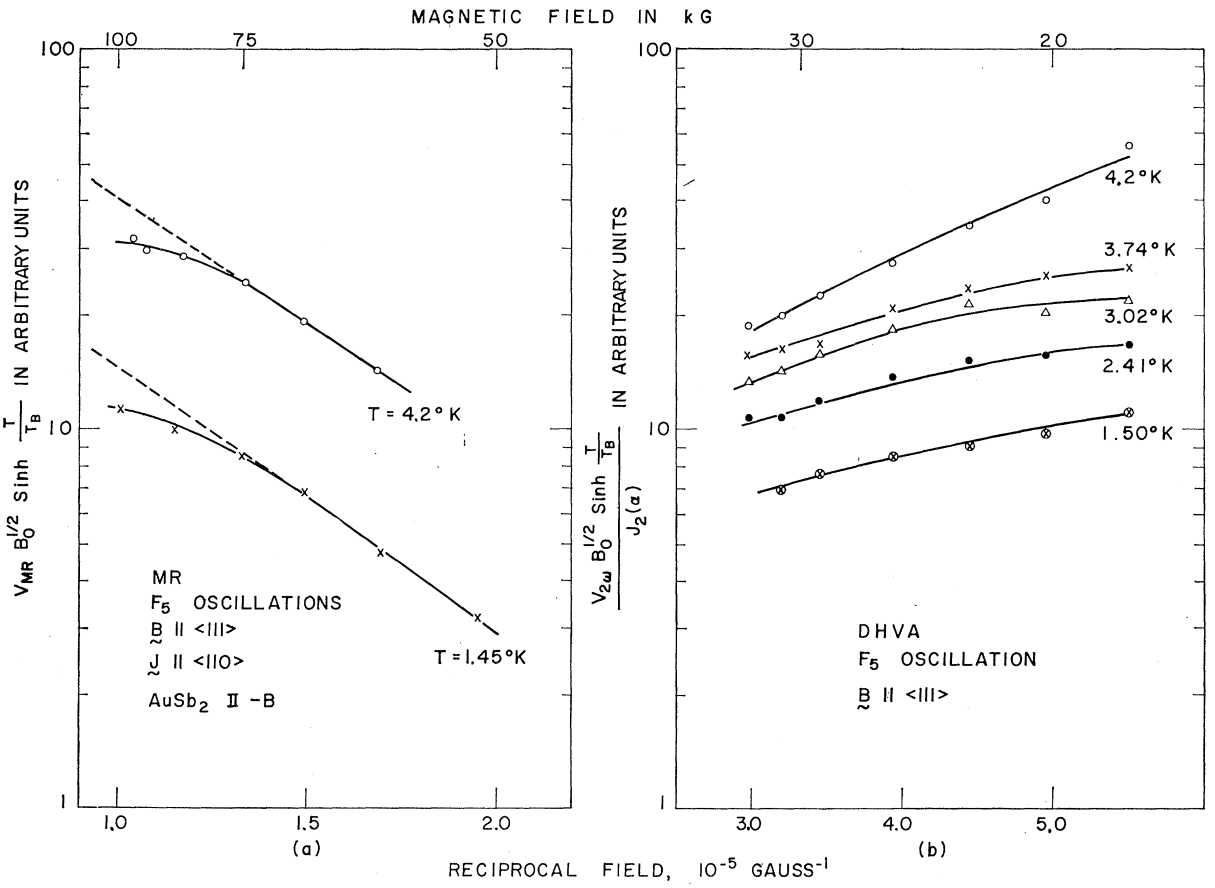

FIG. 8. Field dependence of the amplitude of F_5 oscillations. (a) MR amplitude, data points taken from plots such as Fig. 7(a); (b) dHvA amplitude, data points taken from plots such as Fig. 6. $J_2(\alpha)$ is a second-order Bessel function which arises through the field-modulation technique (see Ref. 34).

experiments. The F_5 oscillations were chosen for study because the amplitude of both types of oscillations was relatively large. Cyclotron masses for F_5 at ⟨110⟩ and ⟨111⟩ were determined in the standard way[12] from the temperature dependence of the amplitude at constant field. The results are as follows: $m_c/m_0=0.19$ (dHS), 0.21 (dHvA), and 0.16 (dHvA) for $\mathbf{B}\|\langle 111\rangle$, ⟨111⟩, and ⟨110⟩ directions, respectively. Thus, within experimental error, the dHS and dHvA effects give identical masses for $\mathbf{B}\|\langle 111\rangle$.

Attempts to determine the Dingle temperature using above masses are shown in Figs. 8(a) and 8(b). In Fig. 8(a), the amplitude first increases with field as predicted by theory but the slope becomes less above ~75 kG. From the linear portion, the Dingle temperatures were determined at $T=4.2°\mathrm{K}$ ($T_D=5.5°\mathrm{K}$) and at $T=1.45°\mathrm{K}$ ($T_D=6.0°\mathrm{K}$). In 8(b), however, the dHvA amplitude does not fit the theory over any portion of the field region investigated, The data for $T=3.74°\mathrm{K}$ were obtained from Fig. 6 which shows that it was not possible to investigate the dHvA amplitude at fields lower than about 16 kG; for $B\lesssim 16$ kG the amplitude becomes rather small and also goes through a series of Bessel function zeroes, one of which occurs at 15.9 kG. From these observations, it is clear that the dHvA amplitude of the F_5 oscillations becomes "anomalous" (i.e., nonlinear as shown in Fig. 8) at fields much lower than 75 kG where the MR amplitude of the same oscillations becomes anomalous. The anomaly in the dHvA amplitude is not restricted to the ⟨111⟩ direction alone. It persists as the field is tipped away from ⟨111⟩ toward ⟨100⟩ in a {110} plane.

V. DISCUSSION

In this section we first discuss the origin of the MR oscillations and the field dependence of the MR and dHvA oscillations for the F_5 oscillation when $\mathbf{B}\|\langle 111\rangle$. The construction of the NFE Fermi-surface model is then described and the predictions of this model are compared with the frequency results.

There are two circumstances that point towards magnetic breakdown as being the cause of the MR oscillations rather than the classical dHS effect as observed in Bi, for example. The first is the apparent loss of *all*

open orbits in fields above about 100 kG as explained in I. The second is the anomalously large amplitude ($\delta\sigma/\sigma\sim\frac{1}{2}$) of some of the MR oscillations. Since $AuSb_2$ is a multiband metal with some fairly large pieces of Fermi surface, it is difficult to understand the magnitude of the MR oscillations except in terms of an effective energy gap, oscillating periodically in inverse field, which essentially turns the open orbits on and off. This mechanism makes a $\delta\sigma/\sigma$ of order unity quite understandable.

It is not surprising, then, that there are deviations in Figs. 8 from the theoretically predicted amplitude behavior. The falloff of the amplitude at high fields from the straight line predicted by theory can be thought of physically as a loss of amplitude due to some of the electrons leaking off the cyclotron orbit in question via the breakdown mechanism. As mentioned in Sec. II B, a falloff similar to that shown in Fig. 8(a) has been observed in the dHvA effect in Zn [25] and a breakdown correction could be applied to the data to bring the curve back to the straight line above the breakdown field. On the basis of the oscillatory MR data in Fig. 8(a) it appears that the characteristic breakdown field B_c for the F_5 oscillations when $\mathbf{B}\|\langle 111\rangle$ is about 75 kG. What is difficult to understand is the complete failure of the theory for the dHvA amplitude in any field range *below* 75 kG where the dHvA oscillations were observed [Fig. 8(b)]. This is especially puzzling since one is obviously observing electrons on the same cyclotron orbits in both experiments. The only qualitative model we have been able to construct which might explain this phenomenon is the following. It is possible that in the reduced-zone scheme, there are two different types of Bragg reflection planes for the cyclotron orbits associated with F_5. At these different types of zone boundaries there could be differing energy gaps. If the open-orbit electrons involved in the MR oscillations must tunnel through the *higher* of the two energy gaps, it might be reasonable that deviations from theory are seen at much higher fields ($\sim$75 kG) in the MR than in the dHvA effect. For the latter, Fig. 8(b) would imply that the characteristic breakdown field for the smaller energy gap is less than 20 kG. Clearly, in order to test the above hypothesis, a good Fermi-surface model is needed to compare the results with a theory such as that of Falicov *et al.*[27,30]

Since magnetic breakdown appears to play an important pole as discussed above and in I, it is necessary to ask whether any of the frequencies shown in Figs. 3 and 4 might be due to cyclotron orbits which exist only as a result of breakdown. These orbits produce dHvA frequencies which arise from sums or differences of true extremal areas of the Fermi surface, as explained, e.g., in Ref. 30. Such combination frequencies can also arise as a result of the *B-H* or magnetic interaction effect.[37] Both of these effects must be considered when one is trying to deduce information about the true Fermi surface of a metal, and, in several instances, such effects have led workers to erroneous conclusions about the Fermi surface. In the case of $AuSb_2$ we have carefully checked the observed frequencies for combinations of other frequencies or harmonics of other frequencies. There are a few instances when certain combinations are equal within experimental error to other observed frequencies but, in these cases, the correspondence does not hold except at isolated angles of the $F(\theta)$,$F(\eta)$ curves. Therefore, for the purposes of the following discussion, it seems reasonable to take all the frequencies shown in Fig. 4 as corresponding to true extremal cross sections of the Fermi surface.

In view of the success enjoyed by the NFE model in polyvalent metals and in a number of metallic compounds based on gold, it seemed worthwhile to construct this model for $AuSb_2$. The primitive cell of $AuSb_2$ contains four $AuSb_2$ units. Each gold and antimony atom was assumed to contribute one and five valence electrons to the conduction bands, respectively. Choosing $2\pi/a$ as the unit length in k space, the Fermi wave vector was $k_F=(33/2\pi)^{1/3}=1.744$. The NFE model was obtained with a computer program[38] which performs the Harrison construction[39] automatically. The computer printouts were the intersections of arbitrary planes with Fermi spheres centered at each reciprocal lattice point. In order to construct three-dimensional models, the computer printouts were made for cross sections of the Fermi spheres parallel to {100}, {110}, and {111} planes which passed through the center of the zone (Γ); also, 10 cross sections were made parallel to {100} in steps of $\pi/10a$ from Γ to X, the midpoint of a zone face. The NFE model for $AuSb_2$ is very complicated and construction of it without the aid of the computer program would have been quite impossible. Perspective drawings of most of the Fermi-surface pieces of the model are exhibited elsewhere[36] but, briefly, the predictions of the NFE model are as follows:

(a) Pieces of Fermi surface exist in 14 Brillouin zones. Of these, the lowest three zones contain hole sheets and the remaining higher zones contain electron sheets. The first two zones contain hole sheets of miniscule size. The third zone contains a hole pocket centered at X and a complicated closed structure of arms. The fourth zone is a large set of interconnected arms which could support open orbits in $\langle 100\rangle$ and $\langle 110\rangle$, and possibly other directions. The fifth zone consists of a large closed "glob" of electrons centered at Γ and a closed electron pocket at R, the cube corner of the zone. The predicted frequencies of these latter two pieces are 4.9 and 2.7×10^7 G, respectively, when $\mathbf{B}\|\langle 100\rangle$. The sixth-zone Fermi surface is a closed electron pocket on the line Δ between Γ and X($F_{100}=8.0+10^6$ G) and a closed electron pocket

[37] See, for example, D. Shoenberg, Can. J. Phys. **46**, 1915 (1968).

[38] We are indebted to J. T. Longo and I. S. Goldstein for writing and adapting this program for $AuSb_2$.

[39] W. A. Harrison, Phys. Rev. **116**, 555 (1959).

at $R(F_{100}=1.9\times10^7$ G). The seventh through fourteenth partially filled zones contain only closed electron pockets centered at R. With $\mathbf{B}\|\langle100\rangle$ the predicted frequencies from these zones range from 2.0 to 11.5×10^6 G. For comparison, a cross-sectional area equal to that of the square face of the Brillouin zone would produce a dHvA frequency of 9.3×10^7 G.

(b) The model predicts 18 extremal cross sections for $\mathbf{B}\|\langle100\rangle$ and 16 extremal cross sections for $\mathbf{B}\|\langle110\rangle$.

(c) Many of the Fermi-surface pieces in neighboring zones are congruent in {100} and {110} planes. That is, extremal areas for $\mathbf{B}\|\langle100\rangle$ and $\langle110\rangle$ predicted for many neighboring zones are the same.

General Fermi-surface properties that can be deduced from the experimental results given in I and in Sec. IV of this paper are as follows:

(a) There exist three nearly spherical pieces of Fermi surface which are closed. These are associated with F_1, F_2, and F_7 in Fig. 4.

(b) There exist three extremal cross sections which apparently arise from rather complicated Fermi-surface geometries; these extrema exist in limited field ranges and are associated with F_3, F_6, and F_8 in Fig. 4.

(c) At least one sheet of Fermi surface is multiply connected so that $\langle100\rangle$, $\langle110\rangle$, and $\langle112\rangle$ open orbits can exist.

(d) The electron and hole volumes of the Fermi surface are equal.

In comparing the model with the experimental results there are several obvious conclusions to be drawn. One is that the observed open orbits do not seem to contradict the model although, for reasons to be made transparent below, we have not investigated in detail the compatibility of the $\langle112\rangle$ open-orbit regions with predictions of the model. Secondly, the model predicts many more extremal cross sections than were observed which, again does not *necessarily* contradict the model. However, if a NFE Fermi-surface model is to have any validity at all as a first approximation, it should be possible to correlate the angular dependence of extremal areas on its *larger* pieces, those for which the lattice should be a small perturbation, with the experimentally observed ones. This we were not able to do. In particular, the model seems to possess no rather large and nearly spherical pieces that could account for the fairly weak angular dependence of F_1 and F_2. Therefore, it appears that the NFE model is not a good approximation to the band structure of $AuSb_2$.

In all the successful applications of the NFE model to pure metals and metallic compounds,[2,4,7,8] it was always assumed that *all* the valence electrons go into the conduction bands: The valence was determined simply by the number of s and p electrons in each element, i.e., by the column of the Periodic Table. While this assumption was justified by demonstrating that experimental result agreed with the NFE predictions, there seems to be no *a priori* reason why this assumption should have universal validity in all "*s-p*" metallic compounds. We have considered therefore a modified NFE model in which it was assumed that one 6*s* electron from each gold atom and three 5*p* electrons from each antimony atom go into the conduction bands. That is, the two 5*s* electrons were regarded as tightly bound core electrons. The only (rather weak) justification for trying such a model is that the 5*s* energy level in atomic antimony is considerably lower ($\sim$0.5 Ry) than the 5*p* level.[40] The calculated atomic levels of all the valence states in question are as follows[40]: $E_{6s}(\mathrm{Au})=-0.4775$ Ry, $E_{5s}(\mathrm{Sb})=-1.0898$ Ry, $E_{5p}(\mathrm{Sb})=-0.5337$ Ry. Therefore, the Au 6*s* electrons and the Sb 5*p* electrons would be expected to mix together in the solid; however, depending upon the exact amount of overlap of the Sb 5*s* electron wave functions, these latter electrons might be essentially tightly bound. Such a modified NFE Fermi-surface model was constructed as described above for comparison with the observed extremal areas. However, as was the case with the earlier model, it was not possible to understand the experimental results on the basis of the model. It seems therefore, that further attempts to understand the Fermi-surface data for $AuSb_2$ will have to await the performance of a first-principles energy-band calculation.

VI. CONCLUSIONS

In the present work we have determined the orientation dependence of eight sets of extremal Fermi-surface cross sections for $AuSb_2$. Some of the details of the MR and dHvA oscillation amplitudes seem to indicate the presence of magnetic breakdown.

The room-temperature resistivity of $AuSb_2$ is 25$\mu\Omega$ cm which, perhaps fortuitously, is approximately the weighted average of the resistivities of its constituents. However, $AuSb_2$ is clearly not a semimetal like Bi or Sb in the sense that its Fermi surface contains several rather large pieces. The largest extremal area observed corresponds roughly to half the area of a cube face of the Brillouin zone. The existence of large pieces of Fermi surface seems, in general, to be a necessary condition for the validity of the NFE approximation. Two NFE Fermi-surface models were constructed but neither was capable of explaining the frequency data. The models assumed a valence of either 5 or 3 for antimony. $AuSb_2$ is known to become superconducting at 0.58°K.[41] It has been found empirically that a necessary condition for superconductivity is[42] $2\leq\bar{N}\leq8$, where $\bar{N}$ is the average number of valence electrons per atom in a metal or

[40] F. Herman and S. Skillman, *Atomic Structure Calculations* (Prentice-Hall, Inc., Englewood Cliffs, N. J., 1963).

[41] B. T. Matthias, T. H. Geballe, and V. B. Compton, Rev. Mod. Phys. **35**, 1 (1963).

[42] B. T. Matthias, in *Progress in Low Temperature Physics* (North-Holland Publishing Co., Amsterdam, 1957), Vol. II, pp. 138–141.

alloy. The two NFE models do satisfy this condition because $\bar{N}$ is 11/3 or 7/3 assuming a valence of 5 or 3 for antimony. Therefore, it cannot be argued that the NFE models fail because they do not have an $\bar{N}$ consistent with superconductivity.

It is clear that there are some systematic quantum chemical trends in $AuSb_2$ and other pyrite structure compounds. Johnston *et al.*[43] have reported electronic properties of a large number of pyrite (and the closely related marcasite) structure compounds. They, and others, have shown that compounds having 20 valence electrons per molecule are semiconductors while those with more are metals. Compounds with less than 20 valence electrons per molecule probably are semiconductors. $AuSb_2$, with 21 electrons, fits into this pattern and it will be interesting to see whether *ab initio* band calculations are able to reproduce the observed electrical properties of this class of solids.

Finally, among all the metallic compounds not containing transition metals which have been investigated to date, $AuSb_2$ is the first one whose Fermi surface deviates significantly from the NFE model based on the normal valences of the constituent atoms. In addition to $AuSb_2$ there are now several other metallic compounds whose Fermi surfaces have been experimentally investigated but are not well understood. These include InBi,[44] tetragonal structure; $MgZn_2$,[45] hexagonal structure; PtSn,[46] nickel arsenide structure; RuO_2,[47] rutile structure; and ZrB_2,[48] hexagonal structure. Some of these structures contain a rather large number of atoms per primitive cell and will provide a stringent test for present energy-band techniques. Augmented-plane-wave calculations have been performed for the β-wolfram structure compound V_3Ga [49] which contains eight atoms per primitive cell. This represents the largest number of atoms per primitive cell which have been treated by one of the first-principles methods. It would appear that among the above poorly understood compounds there is ample opportunity for the development and testing of new approximate methods for electronic structure calculations in solids of intermediate structural complexity.

ACKNOWLEDGMENTS

The authors wish to express their appreciation to I. S. Goldstein and Dr. P. J. Tobin for their assistance in various phases of this work. They are indebted to the staff of the Francis Bitter National Magnet Laboratory at M.I.T. for use of its facilities; in particular, L. G. Rubin was most helpful. The financial support for one of us (J. A.) during the entire period of this work was generously provided by the Resident Graduate Study Program sponsored by the IBM Corporation. Support of this research by the Advanced Research Projects Agency through the Center for Materials Science and Engineering of M.I.T. is gratefully acknowledged.

[43] W. D. Johnston, R. C. Miller, and D. H. Damon, J. Less-Common Metals **8**, 272 (1965).

[44] Y. Shapira, S. J. Williamson, and S. Fischler, Phys. Rev. **144**, 715 (1966); Y. Saito, Sci. Rept. Res. Inst. Tôhoku Univ. **A-1642** (1964); A. C. Thorsen and T. G. Berlincourt, Nature **192**, 959 (1961).

[45] B. W. Veal and J. A. Rayne, Phys. Letters **6**, 12 (1963).

[46] W. N. Cathey and J.-P. Jan, Bull. Am. Phys. Soc. **12**, 702 (1967).

[47] S. M. Marcus, Phys. Letters **28A**, 191 (1968); S. M. Marcus and S. R. Butler, *ibid.* **26A**, 518 (1968); R. T. Slivka and D. N. Langenberg, *ibid.* **28A**, 169 (1968).

[48] J. Piper, J. Phys. Chem. Solids **27**, 1907 (1966).

[49] L. F. Mattheiss, Phys. Rev. **138**, A112 (1965).